Title
Complexity and Opportunities in Liquid Metal Surface Oxides

Journal
Chemistry of Materials, 32(21)

ISSN
0897-4756

Authors
Martin, Andrew
Du, Chuanshen
Chang, Boyce
et al.

Publication Date
2020-11-10

DOI
10.1021/acs.chemmater.0c02047

Peer reviewed

CHEMISTRY OF MATERIALS

pubs.acs.org/cm

Perspective

Complexity and Opportunities in Liquid Metal Surface Oxides†

Andrew Martin, Chuanshen Du, Boyce Chang, and Martin Thuo*

Cite This: *Chem. Mater.* 2020, 32, 9045−9055

Read Online

ACCESS | Metrics & More | Article Recommendations

ABSTRACT: The ability of metal alloys to rapidly oxidize in ambient conditions presents both a challenge and an opportunity. Herein, we focus on opportunities buried in the passivating oxide of liquid metal particles. Recently described subsurface complexity and order present an opportunity to frustrate homogeneous nucleation and, hence, enhanced undercooling. The plasticity of the underlying liquid metal surface offers an autonomously repairing subsurface hence, the lowest E^0 component dominates the surface unless stoichiometrically limited. This plasticity provides an opportunity to synthesize organometallic polymers that *in situ* self-assemble to high aspect ratio nanomaterials. An induced surface speciation implies that, under the appropriate oxidant tension, the oxide thickness and composition can be tuned leading to temperature-dependent composition inversion and so-called chameleon metals. The uniqueness of the demonstrated capabilities points to the need for more exploration of this small but rather complex part of a metal alloy.

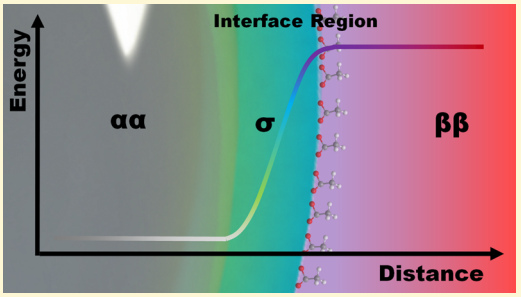

Surfaces and interfaces are ubiquitous across materials. But what is a surface? It depends! For simplicity and brevity, a surface is often defined as the "exterior", "outer boundary", or "termini", hence not part of the material.[1] In this case a surface has no mass and no volume (Gibbs dividing plane, GDP). In other cases, a surface constitutes a continuum of the bulk, only differing by the number density of components (Figure 1a) occupying such a region (Guggenheim Interface, GI). Thermodynamically, surfaces are the *mass* and *energy* dissipation boundary horizons of a system. Defining a surface solely on mass distribution is, therefore, insufficient. Considering energy distribution, the GDP necessitates a duality, in that transition from one phase to the other will constitute a point in space where two values of energy are feasible, that is, an instantaneous jump in energy. This scenario negates any semblance of equilibria and, hence, is unlikely. The GI, on the other hand, with an increasing concentration gradient (Figure 1b), is challenging to understand for low or high cohesive energy density (vapor pressure) material systems. In crystalline materials, however, one can argue that the lattice planes are clearly defined; hence, a GDP is an appropriate descriptor. Considering a flat crystalline metallic system at ambient (pressure jump = 0, vapor pressure ≈ 0) and considering the nature of a metallic bond, then what is on the surface of such a metal? A "sea of electrons" should occupy the surface. From quantum mechanics (uncertainty principle), however, defining the loci of surface electrons negates their flux (speed) across the whole material. On the other hand, assuming an energy gradient (GI) near the surface of an equilibrating mixed material, then autonomous speciation is likely due to curvature, as in the Lowengrub−Voigt model,[2] or in thermo-oxidative composition inversion.[3,4] But what governing rules drives the speciation (Figure 1c)? For reacting components, preferential formation of a bond may lead to order and organization over relatively short distances (1−2 nm) as shown in hydrocarbon self-assembled monolayers (Figure 1d). In more stochastic systems, like formation of passivating oxides on metal alloys (Figure 1a,c), redox-driven differentiation occurs over several nanometers.[5,6] It therefore follows that the surface of a material is a complex part due to its size (nm),[5,7] energy profile,[8] composition, structure, and reactivity.[9] Focusing on the GI, we infer that associated surface tension (γ) is a tensor component derived from the integration of all local speciations over the whole surface (Figure 1e). This equation shows contribution of interfacial excess (Γ_i) for each species (i) and its chemical potential (μ_i) across the surface thickness (x). To understand these ubiquitous parts of metallic materials, we focus on liquid metal systems with an eye on opportunities this complexity provides.

Liquid Metal Particle. Most metals rapidly oxidize in air to form a thin layer of oxide. What is the surface of a metallic particle (Figure 1a)? One can argue that the thin passivating oxide layer makes up the particle surface, but an oxide is not a metal; hence, thermodynamically, it is a different component.

Received: May 15, 2020
Revised: September 12, 2020
Published: September 14, 2020

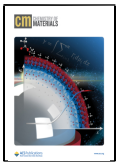

†This Perspective is part of the *Up-and-Coming* series.

https://dx.doi.org/10.1021/acs.chemmater.0c02047
Chem. Mater. 2020, 32, 9045−9055

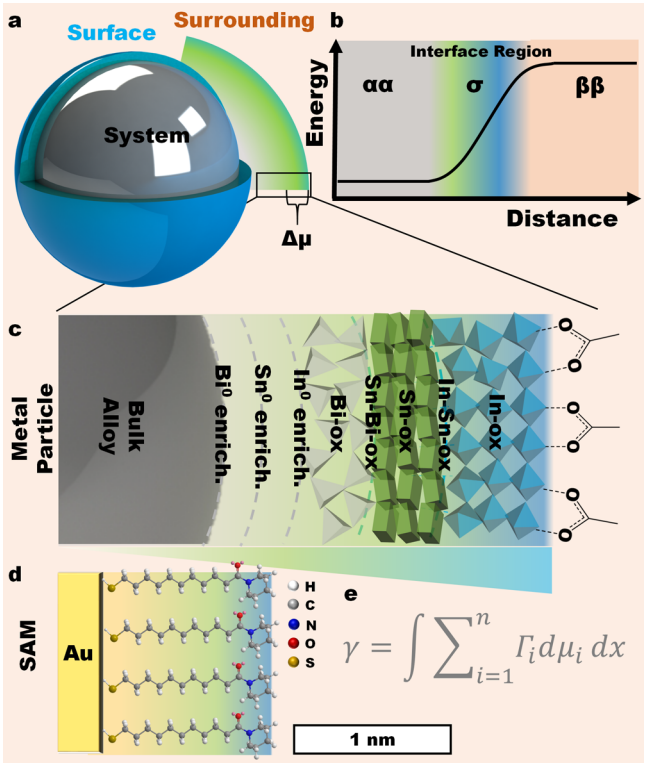

Figure 1. Schematic illustration of energy gradient and matter distribution across a surface oxide. (a) Schematic representation of speciation across the passivating surface layer of a spherical metal particle. (b) Energy profile emanating from the speciation in (a). Structure and dimensional comparison of metal surface oxide, here (c) Field's metal vs (d) a self-assembled monolayer (gray: carbon, yellow: sulfur, white: hydrogen, red: oxygen, blue: nitrogen) on gold. (e) Composite surface tension across the graded Guggenheim interface expressed in terms of species distribution.

So how is this part of the metal, and yet not a component of itself? To define a surface, in this respect, is to look for a set of components that are not part of the object in consideration—and borrowing from set theory, this argument mirrors Russell's paradox.[10−12] It is therefore safe to argue that, though dissimilar, the passivating oxide and the energetically dissimilar interface metal layer constitutes the surface. This definition is analogous to that adopted by others in the understanding of interfaces.[8,13]

Is the passivating oxide then similar to the self-assembled monolayer (SAM) on coinage metals where the organic and the metal are clearly different entities (Figure 1c)? NO! Unlike the monolayer system that has a definitive linkage point, the Au−S bond, for example (Figure 1d), the passivating oxide is a dynamic continuum, emergent from the bulk and a result of an equilibrating system. This relationship would lead to a high-rank tensorial descriptor for surface tension as opposed to the vectorial nature for SAMs (Figure 1c,d). Simplicity in SAMs may, in part, account for why they are widely studied as compared to the surface oxides.[14−19] The governing rules for the establishment of passivating oxide are largely dependent on the environment (temperature, reactive species, pressure, etc.), the reactivity of components of the alloy, cohesive energy density (how well the alloy components like each other), diffusivity (hence, atomic radius), and thermodynamic state of the bulk. In alloys, how does the passivating oxide emerge and what dictates its composition? Is the passivating oxide layer at equilibrium, or is it metastable like in a high vapor pressure liquid (e.g., a drop of water at ambient)? The low vapor pressure of both the metal and the oxide precludes the possibilities for a gradient in concentration which in turn imposes a duality in energy at the metal−oxide interface, suggesting the existence of an energy jump across a plane (GDP). What then is the nature of this interface? It follows that there must be some gradient in composition or energy states as we approach the metal−oxide layer from the oxide or the metal side of the interface (Figure 1b). This simple inference poses a challenge in our understanding of these rather small (0.7−5 nm) parts of a material, yet (from an energy point of view) the gradient provides a "powerhouse" from which the material, as a whole, can be driven to rather unprecedented products or states. The surface, irrespective of the definition adopted, is therefore a metastable region of the material whose energy state(s) can only be averaged from divergence of energy states across each point on the surface. At ambient, a diffuse layer of speciated surface material (σ) mirrors an energy gradient between the system ($\alpha\alpha$) and its surroundings ($\beta\beta$), and we infer that this gradient must be dynamic and highly susceptible to small perturbations (Figure 1b). Based on the standard reduction potential of the underlying components, their propensity to flux, and interaction with other alloy component, an equilibrium state is established. Figure 1c illustrates this behavior for BiInSn (Field's metal). Understanding this surface, therefore, depends on observation of the length scale, time, and their complexity among other properties. But considering that passivating oxides are larger than most SAMs (e.g., oxide of eutectic gallium indium ≈ 2 nm, while a decanethiol SAM ≈ 1 nm), it is surprising that the literature is scant on their studies. A major hindrance to their exploration is likely the lack of appropriate and affordable tools to capture these subtle differences.[8]

Analogy. The SAMs are one peculiar example of thin (nanometer) surface layers on metal surfaces (e.g., Figure 1d) that significantly alters the properties of the material ranging from the work function,[19−21] tribology/wettability,[17,22−25] conductivity,[15,26−29] to plasmonic activity[30,31] among others.[14,16,18,32−34] This material system has been extensively studied since its first introduction in 1946,[35] whereas the passivating oxide has not garnered similar attention. The SAM can be formed via a thermodynamic driven self-assembly process, resulting in a very ordered structure.[36−39] The deposited thin layer of organic material offers great opportunities in more fundamental areas, most notably the structure−property relationship and interfacial phenomena.[16,18,23] As many studies have revealed, the SAM system can be modeled as two interfaces surrounding the bulk (often a hydrocarbon), where each of these three components can be investigated separately by tuning the basic building block, the molecule.[40] The challenge faced by SAM systems, however, is that because of the small size of the molecular component and effect of conformation/molecular orientations, any minor changes in the surface can significantly alter the entire system.[41] Under well-controlled conditions, however, the SAM can be a rather simple system to understand and analyze.[17,23,25] Many scholars have, therefore, utilized SAMs to advance technological platforms or reveal unprecedented molecular behavior.[17,23,25,28,35] The applications of SAMs can be divided into two types, fundamental structure−property studies and applied. Some applications directly utilize the structure−property relationship of the SAM molecule. For

https://dx.doi.org/10.1021/acs.chemmater.0c02047
Chem. Mater. 2020, 32, 9045−9055

example, the monomolecular nature of SAMs leads to their uses in molecular electronics as well as tunable hydrophobic coating.[15,16,28] On the other hand, the highly tunable nature of SAMs makes them a great candidate platform for building/anchoring other components on metal surfaces.[42−45]

Whereas SAMs on metals are extensively studied, emerging almost as an independent subdiscipline, metal passivating oxides have not garnered a similar level of interest. Advances in liquid metals coupled with advances in characterization methods has, however, highlighted the need to understand, and opportunities in, passivating oxide. By comparing advances in SAMs and how interdisciplinary their impact has been, we infer that improved understanding of passivating metal oxides can lead to similar advances in science and impact in functional materials. It is our conviction that the materials community would be equally enriched by a deeper understanding of these nanometer-sized passivating components of metals. Though this is a fledgling field, we illustrate its potential by exploring the limited literature on structure/morphology of the oxides followed by three case studies showcasing their potential uses by limiting our discussion to liquid metals.

PREAMBLE: THE SURFACE OXIDE

Studies of passivating oxide layer on liquid metal particles have been very limited, in part due to challenges in characterization techniques.[8] This difficulty comes primarily from the compositional complexity within the underlying metal oxide interface over a very small distance. This passivating oxide layer, however, when properly formed and/or engineered, provides various advantages to a material.[46−52] Previous works have empirically shown the complex composition of these interfacial layers on a liquid binary alloy, eutectic gallium−indium EGaIn (75.5% Ga, 24.5% In), metal particles (Figure 2a,b).[5−7,53] On an EGaIn particle, the surface is an ordered layer of adventitious organics, a predominantly Ga_2O_3 outer surface below which suboxides of both Ga and In are formed (Figure 2b). The presence of a buried InO_x layer captures the stoichiometric qualified statistical mechanics principle of equaling *a priori* probabilities for both Ga and In to oxidize upon exposure of the bare alloy to an oxidant (Figure 2b).

In nonreacting liquid droplets, curved surfaces of micro- to nano-sized particles bear a sharp energy and compositional gradients, that are largely captured through the interfacial excess, Γ_i (Figure 1b), and the Laplace pressure jump condition ($\Delta P = 2\gamma/r$, where γ is the surface tension and r is the radius of the particle).[54] By definition, this sharp gradient serves the critical purpose of establishing both energy and mechanical equilibria between the particle and the surroundings.[55,56] For metallic droplets, however, exposure to ambient conditions leads to rapid formation of a passivating oxide layer.[7,56] In metallic alloys, differences in redox potential and diffusivity imply that, at time $t = 0$ of exposure to air, the principle of "equal *a priori* probabilities" dictates that all alloy components stochastically oxidize. Immediately after ($t > 0$), a competitive oxidation ensues; hence, the most abundant, lowest standard reduction potential (E^0) and most diffusive component dominate the outer surface of the formed oxide. This process, however, implies that a kinetically resolved self-sorting and speciation[57] occurs, often resulting in the presentation of a unary metal oxide on the surface of metal alloys.[5,6] This sorting/organization is dominated by, but not limited to: E^0, stoichiometry, atomic size, cohesive energy density, atomic flux, oxidant diffusivity, temperature, and

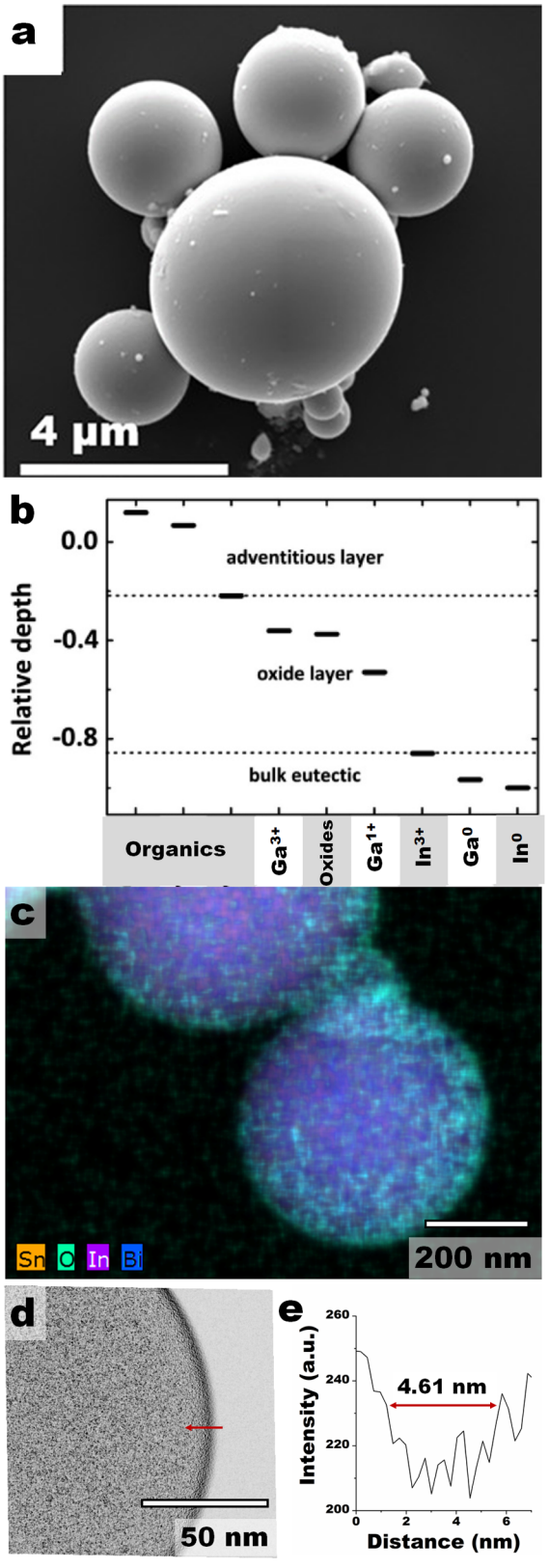

Figure 2. Characteristics of surfaces of liquid metal particles. (a) SEM image of pristine EGaIn particles synthesized using the SLICE method. Reprinted with permission from ref 3. Copyright 2018 American Chemical Society. (b) Depth-dependent distribution of different components across the smooth passivating shell of EGaIn particles determined by XPS. Reprinted with permission from ref 5. Copyright 2012 American Chemical Society. (c) Component distribution map across undercooled Field's metal particles

https://dx.doi.org/10.1021/acs.chemmater.0c02047
Chem. Mater. 2020, 32, 9045−9055

Figure 2. continued

determined using EDS. (d) HAADF-STEM contrast inverted image (Sobel filter) to reveal oxide shell thickness on particles in (c). (e) Line intensity profile perpendicular to the line shown in (d) gives an oxide thickness of *ca.* 4.6 nm for undercooled Field's metal.

pressure.[57−59] Upon reaching a certain critical thickness (d_c^p), oxidation becomes infinitely slow and equilibrium is established (approximately 0.7−5 nm, Figure 2b−e).[58−61]

Given the principle of equal *a priori* probabilities and a thickness-dependent oxidation mechanism from Cabrera−Mott (<20 nm) to Wagner (>1 μm) regimes, speciation becomes a kinetically driven but thickness-limited process. In EGaIn the surface dominant element is gallium under the Cabrera−Mott regime (Figure 2b). Over time, the oxide reaches d_c^p, as flux diminishes, leading to formation of underlying suboxides. For a eutectic, selective depletion of some of the alloy components, albeit small, creates an energetically unfavorable hypoeutectic, which induces enrichment of unreacted components at the metal−oxide interface in a manner that counters/mirrors speciation across the oxide shell (Figures 1c and 2b).[53,62,63] Sharp compositional gradients, however, present an interface with a large chemical potential gradient ($\Delta\mu$), hence, a metastable surface.[64] The $\Delta\mu$ coupled to ΔP presents a divergence in stress that scales inversely with size of the particle. We inferred that such a gradient affects the properties of the said particle in previously unprecedented way(s), akin to the SAM, and, hence, can be tuned to bestow new functions to a metal or drive alternate processing pathways. Below, we illustrate the utility of this high concentration of tension via three dissimilar cases.

CASE 1: METASTABILITY THROUGH SURFACE ASYMMETRY

Based on our inference on asymmetric energy distribution (high $\Delta\mu$) across the surface oxide, it should be possible to perturb the energy landscape (hence relaxation) in the bulk via the passivating layer. Considering that molten metals have high symmetry (no order as defined in Landau's theory),[65−67] formation of passivating oxides and the underlying enrichment to maintain bulk equilibrium (e.g., eutectic composition)

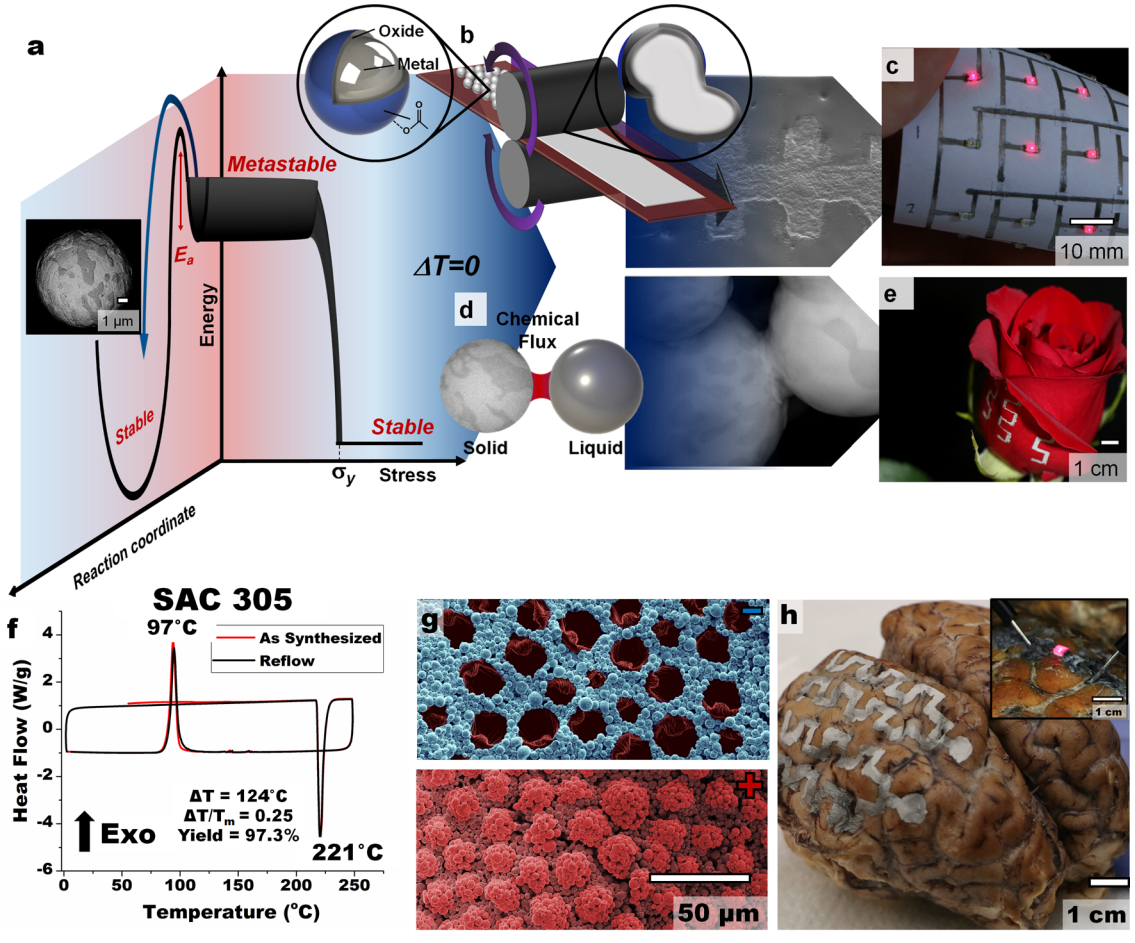

Figure 3. (a) Hypothetical divergence in the energy landscape between solidified and undercooled metal particles. (b) Heat-free mechanical processing of undercooled metal particles and (c) direct writing conductive interconnects on paper using undercooled Field's metal particles. (d) Heat-free chemical sintering of undercooled metal particles to create neck joints, a consequence of the preceding capillary bridges. (e) Conductive lines on a rose petal. Reprinted with permission from ref 86. Copyright 2019 Wiley Publishing. (f) Undercooling of commodity solder, SAC 305, to a liquidus state below 373 K as captured by DSC. (g) (top) Conformal packing and densification of Field's metal particles on surface features of a rose petal enabled by self-filtration, capillary forces, and jamming. (bottom) Sintered solid metal biomimetic replica of a rose surface. Reprinted with permission from ref 90. Copyright 2020 Wiley Publishing. (h) Conformal recoverable conductive traces drawn on a brain surface using undercooled metal particles. Inset: a working LED on these features. Reprinted with permission from ref 91. Copyright 2020 Wiley Publishing.

https://dx.doi.org/10.1021/acs.chemmater.0c02047
Chem. Mater. 2020, 32, 9045−9055

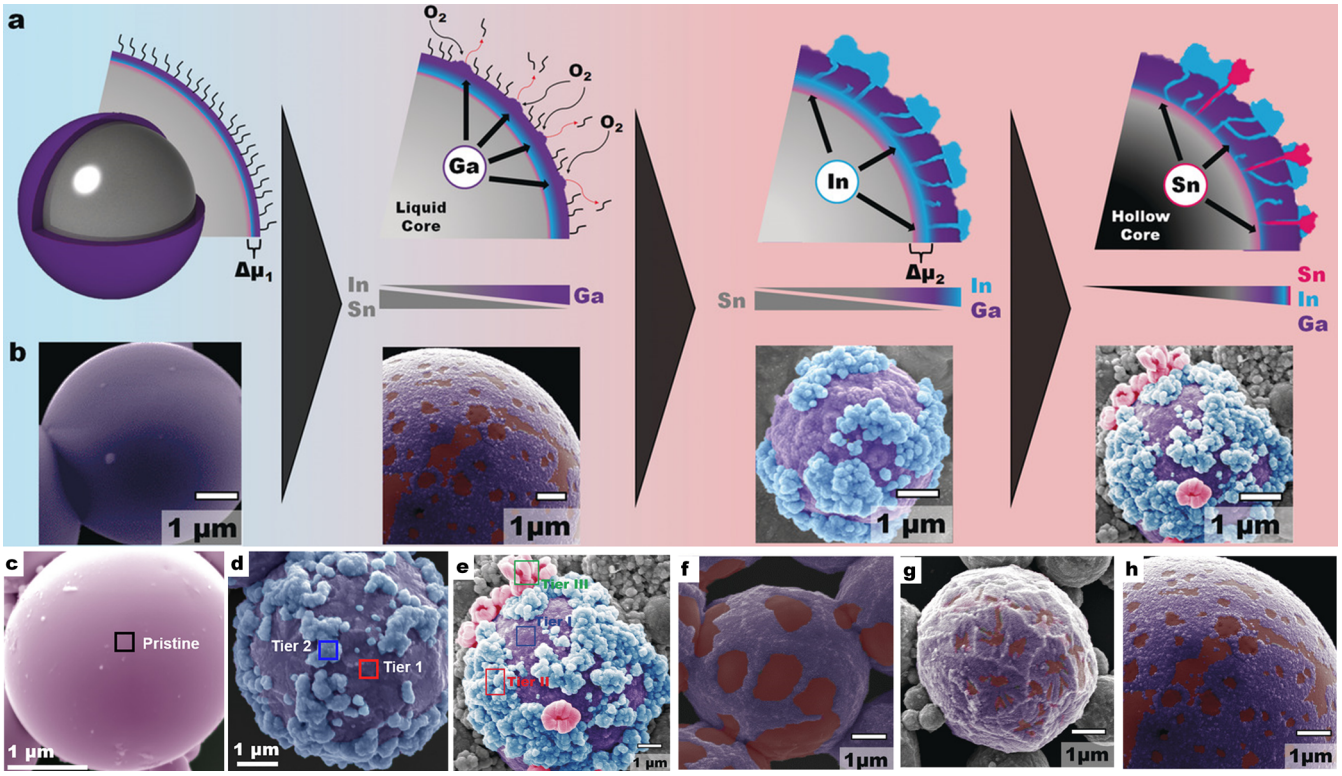

Figure 4. (a) Schematic illustration of the TOCI process on liquid Galinstan particles capturing the tunable release of different elements to the outer surface. (b) SEM images validating the mechanism shown in (a). SEM image of the (c) pristine binary alloy (EGaIn) particle and the (d) EGaIn particle heat treated at 873 K showing only two tiers while (e) a ternary alloy (Galinstan) shows three tiers corresponding to redox differentiation of the principle component on each tier. Fractal patterns for tier 1 derived from (f) gallium, (g) EGaIn, and (h) Galinstan. All these patterns are Ga_2O_3-rich, but stoichiometry dictates volume and organization. Parts (a), (b), and (e)−(h) are reprinted with permission from ref 4. Copyright 2020 Wiley Publishing. Parts (c) and (d) are reprinted with permission from ref 3. Copyright 2018 American Chemical Society.

introduces restrictions on free diffusion in the liquid. Seed nucleant (initial) growth must overcome surface tension—this discussion, however, has failed to incorporate any contributions due to a passivating layer. Even after a nucleant seed forms, a competition between growth (reduction of bulk energy) vs shrinkage (increase in surface energy) ensues with the process getting biased to the former with increase in size. Kelton and Greer observed that although the role of interfacial energy in inhibiting nucleation is empirically known, its origin remains unknown.[68−70] Succinctly, they argue that "*The magnitude of the nucleation rate is extremely sensitive to the value of the interfacial energy, variations in* σ_{ls} *(solid−liquid interface free energy) of only a few percentage can alter the predicted rate by several orders of magnitude*".[68] We concurred with this argument but inferred that a second nondynamic solid−liquid interface, and associated divergence in free energy, exists underneath the passivating oxide layer. This implies that there are two solid−liquid interface free energy perturbations that must be overcome for successful nucleant formation—that is, the nucleant interface and the oxide interface. Unlike the dynamic nucleant seed interface where shrinkage is overcome with growth, the structure of the passivating oxide is fixed and cannot be perturbed by the growing nucleant. It follows that, by engineering the surface oxide *vis-à-vis* miscibility of the bulk (liquid) components, one can significantly affect the growth of a nucleant especially in a microscale (<10 μm diameter) particle. The passivating oxide, therefore, should lead to significant frustration of liquid−solid phase transformation and, hence, enhanced undercooling.

Previously, undercooling has been achieved by minimizing heterogeneous nucleant(s) through, for example, the containerless approach.[71−74] The containerless approach, however, does not remove homogeneous nucleant(s)—a process that results from structural fluctuations in a liquid, and as such does not exploit the nondynamic surface oxide interfacial tension. It is a perturbation of these liquid-phase fluctuations that we infer can lead to extended arrest of the liquid phase below the melting point.

It is also well understood that the smaller the particle, the higher the likelihood of undercooling. This size effect is due to large surface area-to-volume ratio that limits homogeneous nucleation.[75−78] But what is the role of surface architecture in these size-dependent properties? Considering that Gibbs free energy (ΔG) is expressed as $\Delta G = \Delta H - T\Delta S + \delta w'$[64] (here ΔH and ΔS are the change in enthalpy and entropy, respectively, T = temperature, and $\delta w'$ = non-PV work), under the right enthalpy−entropy compensation conditions, surface work ($\delta w'$) can dominate ΔG. While the aforementioned methods rely heavily in tipping the bulk enthalpy−entropy balance to manipulate phase transition,[79−81] $\delta w'$, and in particular surface contributions, is often assumed to be negligible due to entropic limitations. But as inferred above, curved surfaces are metastable and, hence, a source of significant free energy stress (Figure 1c) that can alter the energy landscape of the bulk (Figure 3a).[82−86] We infer that engineering the surface oxide can lead to extension of these size-dependent (surface area-to-volume ratio) properties beyond the nano- into the microscale.

https://dx.doi.org/10.1021/acs.chemmater.0c02047
Chem. Mater. 2020, 32, 9045−9055

The surface work term captures the amount of energy needed to maintain the surface per unit area since $\delta w' = \gamma dA$. Surface tension, by definition, is the product of the interfacial excess and chemical potential difference, $d\gamma = \sum_{i=1}^{n} \Gamma_i d\mu_i$ (Figure 1e).[64] The complex composition gradient demonstrated above creates a large curvature-dependent $\Delta\mu$ gradient; hence, in small particles with large surface areas, the amount of $\delta w'$ can overcome the enthalpy−entropy balance and frustrate the liquid−solid phase transition ($\Delta G_{LS} > 0$), even when these perturbations are small, as observed by Kelton and Greer.[68] But are these perturbations sufficient to overcome thermal fluctuations (thermodynamically, $K_B T$) and, hence, homogeneous nucleant growth for such processed particles to be of practical use? We infer that the structural complexity of the oxide, when properly tuned, can be sufficient as demonstrated by the long-term (years) stability of such prepared particles.[86] Besides the effect on free energy, formation of a uniformly smooth passivating oxide layer forms a physical barrier to heterogeneous nucleant(s) and, hence, enhances the stability of the undercooled state. This understanding enabled the synthesis of stable undercooled liquid metal core−shell (ULMCS) particles enabling heat-free solders and a plethora of other ambient or low-temperature metal processing.[85−89] This recent development in preparation method also allowed undercooling of commercially available lead-free solders, SAC 305, achieving liquidous temperature below 100 °C as shown via DSC (Figure 3f). This level of undercooling enables a low-temperature surface mount and electronic packaging. Since the surface is the main driving force of the metastability, fracture of the oxide shell, whether through mechanical or chemical forces, leads to instantaneous flow, coalescence, and solidification (Figure 3b−e). The elimination of heat in the process allows for more versatile approaches in achieving solidification[85,86] and deposition methods,[86,90,91] as well as more choices in substrates for electronic devices. Possible substrates range from flexible substrates like paper or polymers (Figure 3c) to uneven bio-surfaces like roses (Figure 3e,h).[90,91] Low temperature sintering has also enabled biomimetic "soft" lithography on biological surfaces by exploiting self-filtration, capillary densification, and jamming to create solid metal mimics of biological surfaces (Figure 3g). Soft colloids, whose packed forms can be arrested via phase change, have enabled understanding of granular matter packing and densification, with new insight expected with continued studies. The soft granular property of these ULMCS particles coupled with capillary bridge driven sintering (Figure 3d) also enables printing on uneven surfaces, thus achieving a chemical sintered−mechanically reversible printing of surface electrodes. By exploiting particle size polydispersity, mechanical bonding (conformal packing and jamming) on biological multiscale rough surfaces has been achieved (Figure 3h).[86,90,91]

CASE 2: CHAMELEON METALS AND AUTONOMOUS COMPOSITION INVERSION

The observed compositional gradient in distribution of alloy components across the thin oxide−metal interface implies that, under controlled oxidant tension, the structure, morphology, and distribution of surface oxides can be tuned. When the liquid metal particles/droplets are freshly prepared, a thin (0.7−5 nm) passivating shell is formed. Heating the particle accelerates diffusion and permeability, leading to further oxidation and growth of the oxide layer.[60] A change in the oxidation mechanism is expected with the thickening of the passivating layer with the initial Cabrera−Mott regime leading to growth of the lowest E^0 component onto the smooth initial shell (Figure 4a,b). This process is referred to as Expansion-induced Diffusion-limited Oxidation (EDO).[3] Bulk and interface induced thermal stress (pressure) increases as the oxide shell grows with temperature. The stochastic nature of this oxidation, combined with volumetric change, results in surface texturing upon cooling. At a critical oxide thickness, a significant decline in oxide growth is expected unless this oxide shell becomes significantly porous, leading to a switch in the oxidation mechanism from the Cabrera−Mott to the Wagner regime.[60,92,93] On further heating and thicker oxide, stress is dissipated via fractures as oxide layer yields. Under well controlled oxygen tension, the underlying concentration-differentiated layers effuse through these fractures and oxidize. For brevity, this process is referred to as Thermo-mechanical Fracture leakage and Oxidation (TFO).[3,4] The leakage of materials, therefore, can be tuned to follow the order of the self-sorted composition of the metal interface below the passivating shell. It therefore follows that the released components will be organized according to their E^0 values with the lowest component dominating the EDO regime while the TFO regime is layered in order of increasing reduction potential (Figure 4a,b).[3,4] Finally, at a much higher temperature, complete oxidation of the particle results in a hollow core.[3]

Author: This ansatz has been demonstrated using unary (Ga), binary (eutectic gallium indium, EGaIn), and ternary (Galinstan) systems.[3,4] Figure 4a schematically illustrates the evolution of the surface components and texture with heating for a ternary eutectic alloy, Galinstan. From the smooth equilibrated shell, we observed effusion of the low E^0 Ga in fractal like patterns across the surface of the already Ga-rich smooth surface (Figure 4a,b). For clarity, we false colored the two surfaces to highlight the texture. With increased heating, In-rich and then Sn-rich features emerge (Figure 4a,b). Similarly, with the binary alloy EGaIn the initially smooth gallium oxide rich shell (Figure 4c,d) is transformed.[5,6] These particles undergo EDO and TFO releasing gallium- (tier 1) and indium- (tier 2) enriched exudates to the surface with concomitant surface texturing (Figure 4d).[3,4] We refer to this process as thermo-oxidative composition inversion (TOCI) since buried element in the native oxide shell occupies the highest surface points after TFO. This process continues until majority of the surface is dominated by tier 2 material (indium). As shown with Galinstan (Figure 4e), an increase in number of components in an alloy leads to multiple tiers, from where we infer that this process can potentially continue *ad infinitum*, albeit at different release temperatures to generate patterned surface oxides (tiers), all dominated by a redox-differentiation of alloy components.[4] This kinetic phenomenon is sensitive to temperature and partial pressure of oxygen, but alloy composition (stoichiometry) dictates the proportion of each component. The gradual enrichment and surface patterns derived from TOCI can, therefore, be tuned through alloy design. Figure 4f−h shows changes in surface fractal patterns formed on a unary (Ga), binary (EGaIn, 75% Ga), and ternary (Galinstan, 68.5% Ga) alloys respectively, under approximately the same amount of thermal energy. As the number of elements in an alloy increases, smaller and more segregated features of the same element after EDO are observed. Pure gallium (Figure 4f) forms the largest, and most dense, oxide island structures likely due to unperturbed uniform oxygen and

https://dx.doi.org/10.1021/acs.chemmater.0c02047
Chem. Mater. 2020, 32, 9045−9055

metal diffusion. As the number of components increases, however, atomic interactions between the elements (cohesive energy density) introduces a barrier to free flow (flux), resulting in much smaller and segregated surface oxide features (Figure 4g,h). These results demonstrate that although on a bare alloy surface the principle of equaling *a priori* probabilities dictates a stoichiometry-governed oxidation, once a kinetically resolved thin layer forms, a flux barrier is installed (filter) leading to selective flux of the most reactive component to the surface. This is in line with the Cabrera−Mott oxidation mechanism albeit with the qualification that an initial layer exists for this mechanism to kick in.

We infer that the felicitous choice of alloy composition and thermal treatment conditions provides new pathways to engineer metallic surfaces by introducing desired oxides to the surface, based on differences in E^0 and processing temperature. Not only do the surfaces of these metals change, but they invert under an appropriate thermal (temperature) trigger; hence, we refer to them as "chameleon metals". We believe that the plastically deforming metal surface, coupled with high atomic diffusivity in the liquid, allows the establishment of an organized metal underlayer (beneath the oxide), akin to concentration-driven organization on a GDI, allowing the sequential inversion to occur as described above. This observation serves as indirect evidence that (i) a self-sorting surface oxide is present, and (ii) this surface speciation induces order on the metal layers immediately below the oxide shell; hence, the proposed underlying E^0-driven self-sorting is valid. Relating these observations to case 1 above, one can infer that, depending on the thickness of this organized metal underlayer, the structure of the oxide shell will significantly affect the energy landscape of a metal particle especially with decrease in size. The organization inferred here captures a tension (akin to mirror charges) that must be overcome for any Cahn−Hilliard type diffusion to occur—a necessary condition for nucleation and growth. This work on surface oxidation, therefore, further supports the ability to frustrate nucleant growth, and hence phase transformation, as discussed above.

CASE 3: NANOBEAM SELF-ASSEMBLY

Although the passivating oxides as described above have a rigid order, this is only valid when viewed at their equilibrium state. By having a bridging layer, say between a liquid metal and air, changes in the surroundings can lead to changes in its state, perturbing the established energy gradient. With a liquid core, however, surface plasticity allows the re-establishment of the equilibrium state. This ansatz implies that liquid metal particles, through their oxides, can be a reliable source of specific metal ion(s) even when that component is embedded in an alloy. In a stoichiometrically dictated manner, an alloy can also be used to release metal ions in a predetermined sequence akin to the TOCI process, albeit under an etching (surface subtractive) medium. Since the most reactive components dominate the outer layer of the oxide, it is expected that any process that depletes this element should result in regeneration of a similar surface unless under stoichiometric limitations (i.e., too low of a concentration). Under controlled etching, therefore, the passivating surface oxide generates a controlled flux of atoms from the metal into the surroundings. When the metal ions are only partially soluble in the etching medium, a saturated albeit dilute solution is formed (Figure 5b). The steady state, but low,

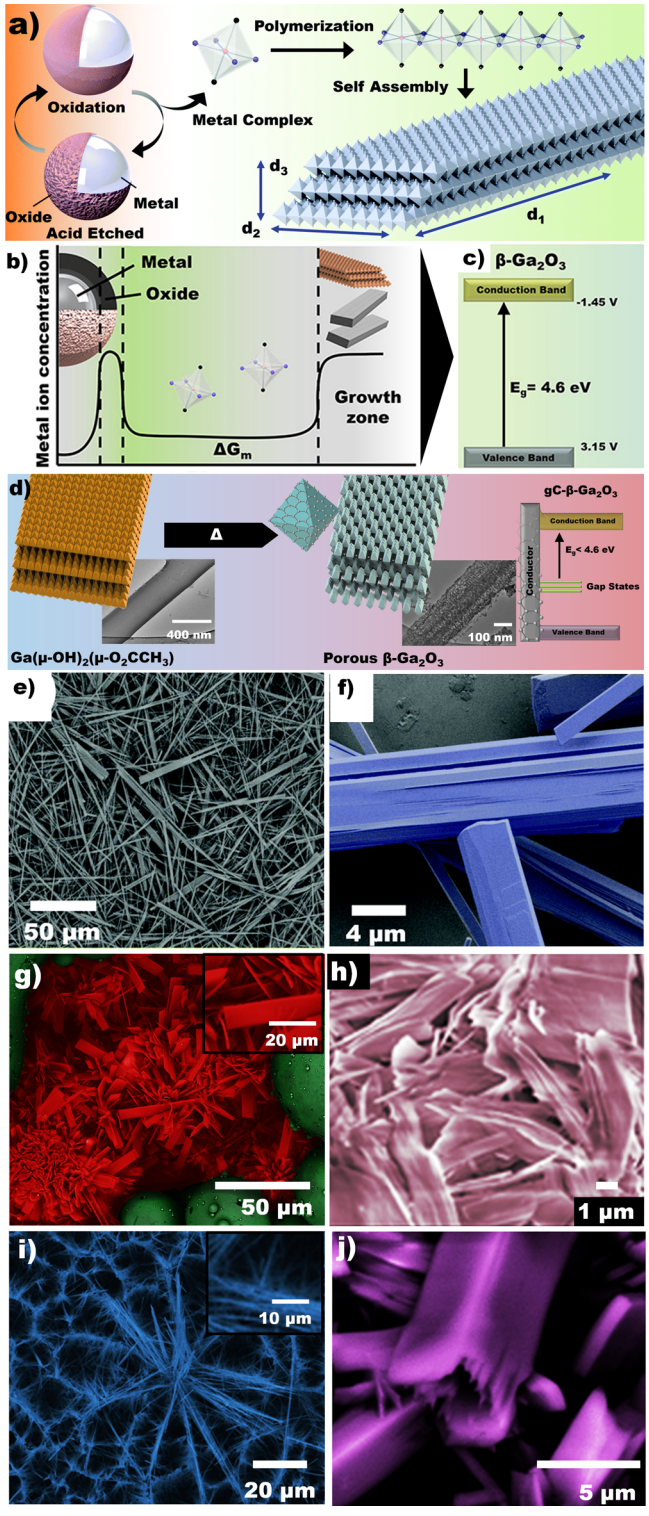

Figure 5. *In situ* heterogeneous metal/ligand (HetMet) reaction for nanobeam synthesis. (a) Schematic illustration of the HetMet process. (b) Concentration profile of the metal ion with radial distance from the metal to the precipitate. (c) Schematic illustration of the band structure of β-Ga_2O_3. (d) Schematic illustration of thermal conversion of assembled Ga-based coordination polymers from (a) into mesoporous graphitic carbon-coated Ga_2O_3 with corresponding transmission electron microscopy (TEM) images of the respective material. Schematic illustration of changes in the Ga_2O_3 band structure [from that in (c)] with the creation of induced gap states is also shown. (e, f) SEM image of synthesized nanobeams. (g, h) Formation of sheet-like structures. (i) Formation of needle-like

https://dx.doi.org/10.1021/acs.chemmater.0c02047
Chem. Mater. 2020, 32, 9045−9055

Figure 5. continued

nanowires and (j) assembly of beams into hollow tubes (gallium oxide). Parts (a), (e), and (f) are reprinted with permission from ref 50. Copyright 2019 Royal Society of Chemistry (licensed under a Creative Commons Attribution-Non Commercial 3.0 Unported License https://creativecommons.org/licenses/by-nc/3.0/, portions of the figure were rearranged and letter indications were changed). Parts (b)−(d) are reprinted with permission from ref 94. Copyright 2020 American Chemical Society.

concentration of the metal ions is ideal for autonomous rate/concentration-dependent processes like polymerization, crystallization, and self-assembly. Through felicitous choice of reactants that act as both etchants and ligands (e.g., a conjugate acid−base pair), *in situ* heterogeneous metal/ligand (HetMet) reaction[50,94] enables steady state synthesis of organometallic (coordination) polymers (Figure 5a). Using an aqueous organic acid, for example, leads to dissociated proton-carboxylate pairs where the proton can etch the metal while the carboxylate chelates the released ions. Where needed, the carboxylate chelated metal center can recruit hydroxyl ligands from the water to saturate its coordination sphere (Figure 5a). Control over the metal ions generated, the stoichiometry, reaction conditions, and the reaction medium can lead to control over the products obtained.[50]

When this process is carried out in a solvent in which the chelated metal ion is sparingly soluble, the metal complexes can self-assemble into one-dimensional coordination polymers that are even less soluble (Figure 5b). Further self-assembly leads to a 3D structure that continues to grow *ad infinitum* (Figure 5a), leading to high aspect ratio materials (Figure 5d−f). By design, the shapes and aspect ratios (d_1, d_2, d_3 in Figure 5a) of these materials can be controlled through polymerization (d_1) or the nature of the secondary interactions driving the self-assembly process (d_2 and d_3). The former is controlled through reaction time while the latter is by engineering the metal coordination sphere—through felicitous choice of metal−ligand pairing. The HetMet derived coordination polymers have dimensions and reaction kinetics that cannot be achieved with traditional batchwise solvothermal methods.[50] The obtained materials assemble into interesting structures, with acetate−base Ga coordination polymers showing ligand interdigitation upon tight packing. The proximity of the terminal methyl groups is ideal for free radical interchain coupling. We inferred that carbonization of the ligands would lead to a carbon coated metal oxide, with the isotropic carbon distribution. The limited number of carbons implied that, in the absence of sintering and given proximity of the ligand, the carbon coating would be graphitic in nature. These self-assembled coordination polymers are, therefore, facile synthons and templates for carbon doping of mesoporous oxides through controlled oxidative ligand ablation. Introduction of a conductor (graphene) on the surface of a semiconductor (oxide) leads to gap induced states to balance the large interface dipole (Figure 5d).[94] This leads to bandgap tunability for various semiconductors and opens them up for unprecedented applications such as catalysis (Figure 5c,d).[94] The ability to perform reactions at ambient conditions permits a larger selection of metal−ligand pairs and, thus, greater control over uniformity of the resulting materials (Figure 5e−j). For example, with slow growth and precipitation, beam-like structures can be obtained (Figure 5e,f). We are continuing to explore the dynamics of this process to enable formation of other morphologies such as sheets [thin (Figure 5g) or wide (Figure 5h)], wires (Figure 5i), or tubes (Figure 5j).

As an interface-controlled reaction, HetMet presents additional design handles during synthesis. The stoichiometry of the metal complexes in solution is a function of the oxide composition, solubility, and selectivity of the ligand. Thus, the final composition of the coordination polymers does not necessarily reflect that of the alloy enabling a "trojan-horse" supply of desired metal ions. Inversely, when the etch rate is significantly high, the speciation on the oxide shell dictates the stoichiometry of the obtained materials, allowing for design of mixed metal coordination polymer precipitates that can then be turned into mixed metal oxides. These mixed oxides, like with the carbon doping, enable isotropic doping of semiconductors, leading to unprecedented properties. By understanding the structure of the surface oxide and its evolution with etching, one can therefore envision programmed multimetal precipitate(s). Where the coordination ligands bear homologous geometries and are not significantly different in size, co-polymerization can be achieved; otherwise, self-sorting occurs, leading to multiple products.[50] In conclusion, we infer that HetMet reactions highlight that subtle changes to the structure of the passivating oxide, under the right reaction conditions, can lead to unique materials in terms of their composition, structure, and self-assembled morphologies. Post-synthesis processing, like selective ligand ablation, leads to unique materials that are realized via an efficient, sustainable, and tunable approach.

■ CONCLUSION/PERSPECTIVE

Passivating oxides, therefore, present unique capabilities that are otherwise impossible to attain. We highlight only three directions that are made possible by the unique structure of the passivating oxide layer, but there is still more to be done. With better understanding, we anticipate that insights in both fundamental know-how and new products will be realized. Specific challenges such as the effect of speciation, in the passivating oxide and at the metal−oxide interface, on the energy landscape of the bulk are yet to be fully quantified. Similarly, *in situ* or direct validation of the inferred oxide-induced inverse speciation/organization on the metal layer(s) immediately below the oxide (Figure 2b) is desired. Dumke and co-workers,[53] coupled with TOCI[3,4] and a simple charge balance (mirror charge due to surface dipole), imply that this is likely. From a free energy point of view, what are the repercussions of such order and how do we quantify it?[16,52] There is a need to understand not only the compositional complexity but also the implications to the free energy landscape across materials, especially with respect to particle dimensions. It is therefore important that we understand the nuances of surface layers with their complexities and opportunities, embracing them as pathways to new material products or efficient processing methods. Extension of this type of thinking to other surfaces and interfaces like grain boundaries can lead to validation of new theories, like the landscape inversion phase transformation theory,[8,13] or inferences derived from them. Herein, we demonstrate synthesis of heat-free solders, coordination polymers, and chameleon metals via simple approaches—but armed with a deeper knowledge of the passivating oxide surface structure.

https://dx.doi.org/10.1021/acs.chemmater.0c02047
Chem. Mater. 2020, 32, 9045−9055

AUTHOR INFORMATION

Corresponding Author

Martin Thuo − *Department of Materials Science & Engineering and Department of Electrical and Computer Engineering, Iowa State University, Ames, Iowa 50011, United States;* orcid.org/0000-0003-3448-8027; Email: mthuo@iastate.edu

Authors

Andrew Martin − *Department of Materials Science & Engineering, Iowa State University, Ames, Iowa 50011, United States*

Chuanshen Du − *Department of Materials Science & Engineering, Iowa State University, Ames, Iowa 50011, United States*

Boyce Chang − *Department of Materials Science & Engineering, University of California, Berkeley, Berkeley, California 94720, United States;* orcid.org/0000-0001-8683-3369

Complete contact information is available at: https://pubs.acs.org/10.1021/acs.chemmater.0c02047

Author Contributions

The manuscript was written through contributions of all authors.

Notes

The authors declare no competing financial interest.

Biographies

Andrew Martin is a Ph.D. candidate in the Department of Materials Science and Engineering at Iowa State University. He received his bachelor's degree in materials engineering at Iowa State University. His research focuses on smart manufacturing and processing techniques with metastable neoteric materials.

Chuanshen Du is a Ph.D. candidate in the Department of Materials Science and Engineering at Iowa State University. He received his bachelor's degree in chemistry and physics at University of Wisconsin—Whitewater. His primary interest is in the surface and interface properties of autonomously assembled systems like organic monolayers and self-aligning nano- or macrosystems.

Boyce Chang is a recent Ph.D. graduate from Prof. Martin Thuo's group at Iowa State University. He is currently a postdoctoral scholar at University of California Berkeley, working under Prof. Ting Xu. His work has previously focused on polymer synthesis with nontraditional systems such as high energy initiators, high pK_a monomers, and application of thermodynamics, rather than kinetics, to control the degree of polymerization.

Martin M. Thuo is an associate professor in the Department of Materials Science and Engineering and in Electrical and Computer Engineering (courtesy) at Iowa State University. Prior to his current position, he was a postdoctoral fellow at Harvard University under the tutelage of Prof. George Whitesides. His research interest is in the interdisciplinary, and emerging, area of frugal science and innovation with a special focus on sustainable engineering through soft matter, surfaces/interfaces, and thermodynamics.

ACKNOWLEDGMENTS

This work was supported by Iowa State University (startup funds to and Black & Veatch faculty Fellowship to MT), Air Force Office of Scientific Research under Award Number FA2386-16-1-4113, and U.S. Department of Energy Award Number DE-SC0018791.

REFERENCES

(1) *Merriam-Webster Dictionary*. Online at http://www.mw.com/home.htm (accessed April 11, 2020).

(2) Lowengrub, J.; Xu, J.; Voigt, A. Surface phase separation and flow in a simple model of multicomponent drops and vesicles. *Fluid Dyn. Mater. Proc.* **2007**, *3* (1), 1−20.

(3) Cutinho, J.; Chang, B. S.; Oyola-Reynoso, S.; Chen, J.; Akhter, S. S.; Tevis, I. D.; Bello, N. J.; Martin, A.; Foster, M. C.; Thuo, M. M. Autonomous Thermal-Oxidative Composition Inversion and Texture Tuning of Liquid Metal Surfaces. *ACS Nano* **2018**, *12* (5), 4744−4753.

(4) Martin, A.; Kiarie, W.; Chang, B.; Thuo, M. Chameleon Metals: Autonomous Nano-Texturing and Composition Inversion on Liquid Metals Surfaces. *Angew. Chem., Int. Ed.* **2020**, *59* (1), 352−357.

(5) Cademartiri, L.; Thuo, M. M.; Nijhuis, C. A.; Reus, W. F.; Tricard, S.; Barber, J. R.; Sodhi, R. N. S.; Brodersen, P.; Kim, C.; Chiechi, R. C.; Whitesides, G. M. Electrical Resistance of Ag^{TS}-$S(CH_2)_{n-1}CH_3$//Ga_2O_3/EGaIn Tunneling Junctions. *J. Phys. Chem. C* **2012**, *116* (20), 10848.

(6) Sodhi, R. N. S.; Brodersen, P.; Cademartiri, L.; Thuo, M.; Nijhuis, C. A. Surface and buried interface slayer studies on challenging structures as studied by ARXPS. *Surf. Interface Anal.* **2017**, *49* (13), 1309−1315.

(7) Farrell, Z. J.; Tabor, C. Control of Gallium Oxide Growth on Liquid Metal Eutectic Gallium/Indium Nanoparticles via Thiolation. *Langmuir* **2018**, *34* (1), 234−240.

(8) Alert, R.; Casademunt, J.; Tierno, P. Landscape-Inversion Phase Transition in Dipolar Colloids: Tuning the Structure and Dynamics of 2D Crystals. *Phys. Rev. Lett.* **2014**, *113* (19), 198301.

(9) Erbil, H. Y. *Surface Chemistry: Of Solid and Liquid Interfaces*; Blackwell Publishing: 2016.

(10) Irvine, A. D.; Deutsch, H. Russell's paradox. In *The Stanford Encyclopedia of Philosophy*; Zalta, E. N., Ed.; Metaphysics Research Lab, Stanford University: Palo Alto, CA, 1995.

(11) Russell, B. Letter to Frege. In *From Frege to Gödel*; van Heijenoort, J., Ed.; Harvard University Press: Cambridge, MA, 1902; pp 124−125.

(12) Russell, B. Appendix B: The Doctrine of Types. In *The Principles of Mathematics*; Russell, B., Ed.; Cambridge University Press: Cambridge, MA, 1903; pp 523−528.

(13) Alert, R.; Tierno, P.; Casademunt, J. Formation of metastable phases by spinodal decomposition. *Nat. Commun.* **2016**, *7*, 13067.

(14) Tao, F.; Bernasek, S. L. Understanding odd- even effects in organic self-assembled monolayers. *Chem. Rev.* **2007**, *107* (5), 1408−1453.

(15) Chen, J.; Gathiaka, S.; Wang, Z.; Thuo, M. Role of Molecular Dipoles in Charge Transport across Large Area Molecular Junctions Delineated Using Isomorphic Self-Assembled Monolayers. *J. Phys. Chem. C* **2017**, *121* (43), 23931−23938.

(16) Chen, J.; Giroux, T. J.; Nguyen, Y.; Kadoma, A. A.; Chang, B. S.; VanVeller, B.; Thuo, M. M. Understanding interface (odd−even) effects in charge tunneling using a polished EGaIn electrode. *Phys. Chem. Chem. Phys.* **2018**, *20* (7), 4864−4878.

(17) Chen, J.; Wang, Z.; Oyola-Reynoso, S.; Gathiaka, S. M.; Thuo, M. Limits to the effect of substrate roughness or smoothness on the odd−even effect in wetting properties of n-alkanethiolate monolayers. *Langmuir* **2015**, *31* (25), 7047−7054.

(18) Love, J. C.; Estroff, L. A.; Kriebel, J. K.; Nuzzo, R. G.; Whitesides, G. M. Self-Assembled Monolayers of Thiolates on Metals as a Form of Nanotechnology. *Chem. Rev.* **2005**, *105* (4), 1103−1170.

(19) Campbell, I. H.; Rubin, S.; Zawodzinski, T. A.; Kress, J. D.; Martin, R. L.; Smith, D. L.; Barashkov, N. N.; Ferraris, J. P. Controlling Schottky energy barriers in organic electronic devices using self-assembled monolayers. *Phys. Rev. B: Condens. Matter Mater. Phys.* **1996**, *54* (20), R14321−R14324.

(20) Crivillers, N.; Liscio, A.; Di Stasio, F.; Van Dyck, C.; Osella, S.; Cornil, D.; Mian, S.; Lazzerini, G.; Fenwick, O.; Orgiu, E.; et al. Photoinduced work function changes by isomerization of a densely packed azobenzene-based SAM on Au: a joint experimental and

theoretical study. *Phys. Chem. Chem. Phys.* **2011**, *13* (32), 14302−14310.
(21) Zehner, R. W.; Parsons, B. F.; Hsung, R. P.; Sita, L. R. Tuning the Work Function of Gold with Self-Assembled Monolayers Derived from X-$[C_6H_4$-C⋮C-$]_nC_6H_4$-SH (n = 0, 1, 2; X = H, F, CH_3, CF_3, and OCH_3). *Langmuir* **1999**, *15* (4), 1121−1127.
(22) Jiang, L.; Sangeeth, C. S.; Yuan, L.; Thompson, D.; Nijhuis, C. A. One-nanometer thin monolayers remove the deleterious effect of substrate defects in molecular tunnel junctions. *Nano Lett.* **2015**, *15* (10), 6643−6649.
(23) Chen, J.; Wang, Z.; Oyola-Reynoso, S.; Thuo, M. M. Properties of Self-Assembled Monolayers Revealed via Inverse Tensiometry. *Langmuir* **2017**, *33* (47), 13451−13467.
(24) Wang, Z.; Chen, J.; Gathiaka, S. M.; Oyola-Reynoso, S.; Thuo, M. Effect of Substrate Morphology on the Odd−Even Effect in Hydrophobicity of Self-Assembled Monolayers. *Langmuir* **2016**, *32* (40), 10358−10367.
(25) Chen, J.; Chang, B.; Oyola-Reynoso, S.; Wang, Z.; Thuo, M. Quantifying Gauche Defects and Phase Evolution in Self-Assembled Monolayers through Sessile Drops. *ACS omega* **2017**, *2* (5), 2072−2084.
(26) Wang, D.; Fracasso, D.; Nurbawono, A.; Annadata, H. V.; Sangeeth, C. S.; Yuan, L.; Nijhuis, C. A. Tuning the Tunneling Rate and Dielectric Response of SAM-Based Junctions via a Single Polarizable Atom. *Adv. Mater.* **2015**, *27* (42), 6689−6695.
(27) Kong, G. D.; Jin, J.; Thuo, M.; Song, H.; Joung, J. F.; Park, S.; Yoon, H. J. Elucidating the role of molecule−electrode interfacial defects in charge tunneling characteristics of large-area junctions. *J. Am. Chem. Soc.* **2018**, *140* (38), 12303−12307.
(28) Chen, J.; Kim, M.; Gathiaka, S.; Cho, S. J.; Kundu, S.; Yoon, H. J.; Thuo, M. M. Understanding Keesom Interactions in Monolayer-Based Large-Area Tunneling Junctions. *J. Phys. Chem. Lett.* **2018**, *9* (17), 5078−5085.
(29) Nijhuis, C. A.; Reus, W. F.; Whitesides, G. M. Molecular rectification in metal-SAM-metal oxide-metal junctions. *J. Am. Chem. Soc.* **2009**, *131* (49), 17814−17827.
(30) Tan, S. F.; Wu, L.; Yang, J. K.; Bai, P.; Bosman, M.; Nijhuis, C. A. Quantum plasmon resonances controlled by molecular tunnel junctions. *Science* **2014**, *343* (6178), 1496−1499.
(31) Du, W.; Wang, T.; Chu, H.-S.; Nijhuis, C. A. Highly efficient on-chip direct electronic−plasmonic transducers. *Nat. Photonics* **2017**, *11* (10), 623−627.
(32) Chen, J.; Liu, J.; Tevis, I. D.; Andino, R. S.; Miller, C. M.; Ziegler, L. D.; Chen, X.; Thuo, M. M. Spectroscopic evidence for the origin of odd−even effects in self-assembled monolayers and effects of substrate roughness. *Phys. Chem. Chem. Phys.* **2017**, *19* (10), 6989−6995.
(33) Thompson, D.; Nijhuis, C. A. Even the odd numbers help: failure modes of SAM-based tunnel junctions probed via odd-even effects revealed in synchrotrons and supercomputers. *Acc. Chem. Res.* **2016**, *49* (10), 2061−2069.
(34) Nijhuis, C. A.; Reus, W. F.; Siegel, A. C.; Whitesides, G. M. A molecular half-wave rectifier. *J. Am. Chem. Soc.* **2011**, *133* (39), 15397−15411.
(35) Bigelow, W. C.; Pickett, D. L.; Zisman, W. A. Oleophobic monolayers: I. Films adsorbed from solution in non-polar liquids. *J. Colloid Sci.* **1946**, *1* (6), 513−538.
(36) Laibinis, P. E.; Whitesides, G. M.; Allara, D. L.; Tao, Y. T.; Parikh, A. N.; Nuzzo, R. G. Comparison of the structures and wetting properties of self-assembled monolayers of n-alkanethiols on the coinage metal surfaces, copper, silver, and gold. *J. Am. Chem. Soc.* **1991**, *113* (19), 7152−7167.
(37) Whitesides, G. M.; Grzybowski, B. Self-Assembly at All Scales. *Science* **2002**, *295* (5564), 2418.
(38) Ulman, A. Formation and Structure of Self-Assembled Monolayers. *Chem. Rev.* **1996**, *96* (4), 1533−1554.
(39) Rusu, P. C.; Giovannetti, G.; Brocks, G. Dipole Formation at Interfaces of Alkanethiolate Self-assembled Monolayers and Ag(111). *J. Phys. Chem. C* **2007**, *111* (39), 14448−14456.
(40) Graupe, M.; Takenaga, M.; Koini, T.; Colorado, R.; Lee, T. R. Oriented Surface Dipoles Strongly Influence Interfacial Wettabilities. *J. Am. Chem. Soc.* **1999**, *121* (13), 3222−3223.
(41) Wang, Z.; Chen, J.; Oyola-Reynoso, S.; Thuo, M. The Porter-Whitesides Discrepancy: Revisiting Odd-Even Effects in Wetting Properties of n-Alkanethiolate SAMs. *Coatings* **2015**, *5* (4), 1034.
(42) Arya, S. K.; Solanki, P. R.; Singh, R. P.; Pandey, M. K.; Datta, M.; Malhotra, B. D. Application of octadecanethiol self-assembled monolayer to cholesterol biosensor based on surface plasmon resonance technique. *Talanta* **2006**, *69* (4), 918−926.
(43) Chaki, N. K.; Vijayamohanan, K. Self-assembled monolayers as a tunable platform for biosensor applications. *Biosens. Bioelectron.* **2002**, *17* (1), 1−12.
(44) Chong, L.-W.; Chien, H.-T.; Lee, Y.-L. Assembly of CdSe onto mesoporous TiO2 films induced by a self-assembled monolayer for quantum dot-sensitized solar cell applications. *J. Power Sources* **2010**, *195* (15), 5109−5113.
(45) Freire, R. S.; Kubota, L. T. Application of self-assembled monolayer-based electrode for voltammetric determination of copper. *Electrochim. Acta* **2004**, *49* (22), 3795−3800.
(46) Dickey, M. D. Stretchable and Soft Electronics using Liquid Metals. *Adv. Mater.* **2017**, *29* (27), 1606425.
(47) Dickey, M. D. Emerging Applications of Liquid Metals Featuring Surface Oxides. *ACS Appl. Mater. Interfaces* **2014**, *6* (21), 18369−18379.
(48) Dickey, M. D.; Chiechi, R. C.; Larsen, R. J.; Weiss, E. A.; Weitz, D. A.; Whitesides, G. M. Eutectic Gallium-Indium (EGaIn): A Liquid Metal Alloy for the Formation of Stable Structures in Microchannels at Room Temperature. *Adv. Funct. Mater.* **2008**, *18* (7), 1097−1104.
(49) Esrafilzadeh, D.; Zavabeti, A.; Jalili, R.; Atkin, P.; Choi, J.; Carey, B. J.; Brkljača, R.; O'Mullane, A. P.; Dickey, M. D.; Officer, D. L.; MacFarlane, D. R.; Daeneke, T.; Kalantar-Zadeh, K. Room temperature CO2 reduction to solid carbon species on liquid metals featuring atomically thin ceria interfaces. *Nat. Commun.* **2019**, *10* (1), 865.
(50) Chang, B. S.; Thomas, B.; Chen, J.; Tevis, I. D.; Karanja, P.; Çınar, S.; Venkatesh, A.; Rossini, A. J.; Thuo, M. M. Ambient synthesis of nanomaterials by in situ heterogeneous metal/ligand reactions. *Nanoscale* **2019**, *11* (29), 14060−14069.
(51) Wang, D.; Wang, X.; Li, Z.; Chi, M.; Li, Y.; Liu, Y.; Yin, Y. Migration of Iron Oxide Nanoparticle through a Silica Shell by the Redox-Buffering Effect. *ACS Nano* **2018**, *12* (11), 10949−10956.
(52) Zavabeti, A.; Ou, J. Z.; Carey, B. J.; Syed, N.; Orrell-Trigg, R.; Mayes, E. L. H.; Xu, C.; Kavehei, O.; O'Mullane, A. P.; Kaner, R. B.; Kalantar-Zadeh, K.; Daeneke, T. A liquid metal reaction environment for the room-temperature synthesis of atomically thin metal oxides. *Science* **2017**, *358* (6361), 332.
(53) Dumke, M. F.; Tombrello, T. A.; Weller, R. A.; Housley, R. M.; Cirlin, E. H. Sputtering of the gallium-indium eutectic alloy in the liquid phase. *Surf. Sci.* **1983**, *124* (2), 407−422.
(54) Israelachvili, J. N. *Intermolecular and Surface Forces*; Academic Press: 2011.
(55) Bormashenko, E. Y. *Wetting of Real Surfaces*; de Gruyter: Berlin, 2013; Vol. *19*.
(56) Butt, H.-J.; Graf, K.; Kappl, M. *Physics and Chemistry of Interfaces*; 3rd ed.; Wiley-VCH: 2013.
(57) Wang, L.-L.; Johnson, D. D. Predicted Trends of Core-Shell Preferences for 132 Late Transition-Metal Binary-Alloy Nanoparticles. *J. Am. Chem. Soc.* **2009**, *131* (39), 14023−14029.
(58) Cabrera, N.; Mott, N. F. Theory of the oxidation of metals. *Rep. Prog. Phys.* **1949**, *12* (1), 163−184.
(59) Saunders, S. R. J.; Monteiro, M.; Rizzo, F. The oxidation behaviour of metals and alloys at high temperatures in atmospheres containing water vapour: A review. *Prog. Mater. Sci.* **2008**, *53* (5), 775−837.
(60) Law, J. T. The High Temperature Oxidation of Silicon. *J. Phys. Chem.* **1957**, *61* (9), 1200−1205.
(61) Over, H.; Seitsonen, A. P. Oxidation of Metal Surfaces. *Science* **2002**, *297* (5589), 2003−2005.

https://dx.doi.org/10.1021/acs.chemmater.0c02047
Chem. Mater. 2020, 32, 9045−9055

(62) Regan, M. J.; Tostmann, H.; Pershan, P. S.; Magnussen, O. M.; DiMasi, E.; Ocko, B. M.; Deutsch, M. X-ray study of the oxidation of liquid-gallium surfaces. *Phys. Rev. B: Condens. Matter Mater. Phys.* **1997**, *55* (16), 10786−10790.
(63) Tostmann, H.; DiMasi, E.; Ocko, B. M.; Deutsch, M.; Pershan, P. S. X-ray studies of liquid metal surfaces. *J. Non-Cryst. Solids* **1999**, *250*−*252*, 182−190.
(64) Jiang, Q.; Wen, Z. *Thermodynamics of Materials*; Springer: Berlin, 2011; p 300.
(65) Wang, C.; Smith, S. Landau theory of the size-driven phase transition in ferroelectrics. *J. Phys.: Condens. Matter* **1995**, *7* (36), 7163.
(66) McMillan, W. Landau theory of charge-density waves in transition-metal dichalcogenides. *Phys. Rev. B* **1975**, *12* (4), 1187.
(67) McMillan, W. Time-dependent Landau theory for the smectic-A-nematic phase transition. *Phys. Rev. A: At., Mol., Opt. Phys.* **1974**, *9* (4), 1720.
(68) Kelton, K. F.; Greer, A. L. Ordering and crystal nucleation in undercooled melts. In *Solidification of Containerless Undercooled Melts*; Herlach, D., Matson, D., Eds.; Wiley-VCH Verlag & Co.: Weinheim, Germany, 2012; pp 87−111.
(69) Palberg, T. Crystallization kinetics of repulsive colloidal spheres. *J. Phys.: Condens. Matter* **1999**, *11* (28), R323.
(70) Kelton, K. *Solid State Physics*; Academic Press: New York, 1991.
(71) Devaud, G.; Turnbull, D. Undercooling of molten silicon. *Appl. Phys. Lett.* **1985**, *46* (9), 844−845.
(72) Devaud, G.; Turnbull, D. Undercooling of Liquid Germanium. *Mater. Res. Soc. Symp. Proc.* **1985**, *57*, 89.
(73) Herlach, D. M. Containerless Undercooling and Solidification of Pure Metals. *Annu. Rev. Mater. Sci.* **1991**, *21* (1), 23−44.
(74) Herlach, D. M.; Cochrane, R. F.; Egry, I.; Fecht, H. J.; Greer, A. L. Containerless processing in the study of metallic melts and their solidification. *Int. Mater. Rev.* **1993**, *38* (6), 273−347.
(75) Perepezko, J. H.; Paik, J. S. Thermodynamic properties of undercooled liquid metals. *J. Non-Cryst. Solids* **1984**, *61*−*62*, 113−118.
(76) Perepezko, J. H.; Paik, J. S. Undercooling Behavior of Liquid Metals. *MRS Symp. Proc.* **1981**, *8*, 49.
(77) Perepezko, J. H.; Wilde, G. Melt undercooling and nucleation kinetics. *Curr. Opin. Solid State Mater. Sci.* **2016**, *20* (1), 3−12.
(78) Herlach, D. M. Non-Equilibrium Solidification of Undercooled Metallic Melts. *Metals* **2014**, *4* (2), 196−234.
(79) Hofmann, D. C.; Roberts, S. N. Microgravity metal processing: from undercooled liquids to bulk metallic glasses. *npj Microgravity* **2015**, *1* (1), 15003.
(80) Perepezko, J. H. Nucleation in undercooled liquids. *Mater. Sci. Eng.* **1984**, *65* (1), 125−135.
(81) Perepezko, J. H. R. D. H.; Anderson, I. E.; Loper, C. R., Jr. *Undercooling of Low-Melting Metals and Alloys*; Metals Society: London, 1979; pp 169−174.
(82) Couchman, P. R.; Jesser, W. A. On the thermodynamics of surfaces. *Surf. Sci.* **1973**, *34* (2), 212−224.
(83) Duhem, P. *Commentary on the principles of thermodynamics by Pierre Duhem*, 1st ed.; Springer: Dordrecht, 2011; Vol. *277*.
(84) Zangwill, A. *Physics at Surfaces*; Cambridge University Press: Cambridge, 1988.
(85) Çınar, S.; Tevis, I. D.; Chen, J.; Thuo, M. Mechanical Fracturing of Core-Shell Undercooled Metal Particles for Heat-Free Soldering. *Sci. Rep.* **2016**, *6*, 21864.
(86) Martin, A.; Chang, B. S.; Martin, Z.; Paramanik, D.; Frankiewicz, C.; Kundu, S.; Tevis, I. D.; Thuo, M. Heat-Free Fabrication of Metallic Interconnects for Flexible/Wearable Devices. *Adv. Funct. Mater.* **2019**, *29* (40), 1903687.
(87) Chang, B. S.; Tutika, R.; Cutinho, J.; Oyola-Reynoso, S.; Chen, J.; Bartlett, M. D.; Thuo, M. M. Mechanically triggered composite stiffness tuning through thermodynamic relaxation (ST3R). *Mater. Horiz.* **2018**, *5* (3), 416−422.
(88) Tevis, I. D.; Newcomb, L. B.; Thuo, M. Synthesis of Liquid Core−Shell Particles and Solid Patchy Multicomponent Particles by Shearing Liquids Into Complex Particles (SLICE). *Langmuir* **2014**, *30* (47), 14308−14313.
(89) Chang, B. S.; Fratzl, M.; Boyer, A.; Martin, A.; Ahrenholtz, H. C.; De Moraes, I.; Bloch, J.-F.; Dempsey, N. M.; Thuo, M. M. Rapid Prototyping of Reconfigurable Microfluidic Channels in Undercooled Metal Particle-Elastomer Composites. *Ind. Eng. Chem. Res.* **2019**, *58* (10), 4137−4142.
(90) Chang, J. J.; Martin, A.; Du, C.; Pauls, A.; Thuo, M. M. Heat-Free Biomimetic Metal Molding on Soft Substrates. *Angew. Chem., Int. Ed.* **2020**, *59*, 16346.
(91) Martin, A.; Du, C.; Pauls, A. M.; Ward, T.; Thuo, M. Polydispersity-Driven Printing of Conformal Solid Metal Traces on Non-Adhering Biological Surfaces. *Adv. Mater. Interfaces* **2020**, 2001294.
(92) Xu, Z.; Rosso, K. M.; Bruemmer, S. Metal oxidation kinetics and the transition from thin to thick films. *Phys. Chem. Chem. Phys.* **2012**, *14* (42), 14534−14539.
(93) Atkinson, A. Wagner theory and short circuit diffusion. *Mater. Sci. Technol.* **1988**, *4* (12), 1046−1051.
(94) Chang, B. S.; Martin, A.; Thomas, B.; Li, A.; Dorn, R. W.; Gong, J.; Rossini, A. J.; Thuo, M. M. Synthesis of Interface-Driven Tunable Bandgap Metal Oxides. *ACS Mater. Lett.* **2020**, *2* (9), 1211−1217.

https://dx.doi.org/10.1021/acs.chemmater.0c02047
Chem. Mater. 2020, 32, 9045−9055